IEEE Access
Multidisciplinary | Rapid Review | Open Access Journal

Received February 4, 2021, accepted February 10, 2021, date of publication March 12, 2021, date of current version June 22, 2021.

Digital Object Identifier 10.1109/ACCESS.2021.3063792

Modeling and Analysis of Offshore Crane Retrofitted With Cable-Driven Inverted Tetrahedron Mechanism

SHENGHAI WANG[1,2], ZHAOPENG REN[1], GUOLIANG JIN[1], AND HAIQUAN CHEN[1,2]

[1]College of Marine Engineering, Dalian Maritime University, Dalian 116026, China
[2]National Center for International Research of Subsea Engineering Technology and Equipment, Dalian Maritime University, Dalian 116026, China

Corresponding author: Shenghai Wang (shenghai_wang@dlmu.edu.cn)

This work was supported in part by the National Key Research and Development Program of China under Grant 2018YFC0309003, in part by the National Natural Science Foundation of China under Grant 51779026 and Grant 51079013, and in part by the China Fundamental Research Funds for the Central Universities under Grant 3132019368.

ABSTRACT Crane operations might be very dangerous in rough sea conditions due to unexpected payload swing induced by ship excitations. In this paper, a novel Cable-Driven Inverted Tetrahedron Mechanism (CDITM) is presented to suppress the payload swing for sake of the workers' safety. The CDITM retrofitting on an offshore crane is simplified as a constrained pendulum with a moving base, and its equations of motion are obtained by Newton Euler Method. Next, three-dimensional dynamic analysis is performed using Matlab/Simulink, and the influence law of ship excitations, tagline tension, crane pose and CDITM configuration on the payload swing are investigated. Finally, through comparative experimental verification, it is found that the simulation tendencies of in-plane swing follows the experiment curves quite well, and the variations between the simulation and experiment results are acceptable. Thus the dynamic modeling and analysis of CDITM are verified. The theoretical and experimental results are fundamental and valuable for the engineering application of CDITM in the offshore industries.

INDEX TERMS Offshore cranes, anti-swing system, payload swing suppression, dynamics.

I. INTRODUCTION

Crane operations in the offshore industries are of great importance, widely used for cargo handling, pipe installation, replenishment, and so forth. During the operations, wave induced ship motions may cause a swing motion of the crane suspended payload. The payload swing will heavily reduce the efficiency of the operations and put the workers nearby in danger. Thus, it is crucial to predict and suppress the payload swing under ship excitations.

In the literature, extensive studies has been done on payload swing control of various cranes, developing control methods like input shaping [1], sliding mode control [2], [3], nonlinear control [4], [5], and so on. Meanwhile, many researchers have been focus on the dynamics of cranes since 1990s and proposed different modeling methods to describe their behaviors in the air [6], [7] or in the waves [8], [9]. The crane models can be divided into three main categories: single pendulum, double pendulum, and constrained pendulum cranes.

There are two classes of models for single pendulum cranes, depending on the way the hoist cable is modeled, namely distributed-mass and lumped-mass models. For the former, the hoist cable is treated as a distributed-mass cable. Meanwhile, the payload and hook are modeled as a point mass and enforced as a boundary condition to this distributed-mass system. Novel [10], [11] built a linearized planar model for a gantry crane. In their study, the wave equation was used to model the hoist cable as a perfectly inextensible, flexible body. In a lumped mass model, the hoist cable is modeled as a massless cable while the payload and the hook is lumped as a point mass. Several dynamic models have been built for different cranes based on the lumped-mass approach, including modeling of an overhead crane [12], [13], modeling of a gantry crane [14], [15], modeling of a rotary crane [16] and offshore container crane [17] by the Lagrangian method, modeling of an offshore hydraulic crane [18] and modeling of a telescopic type rotary crane [19], [20] using the bond graph

The associate editor coordinating the review of this manuscript and approving it for publication was Giambattista Gruosso.

method, and modeling of a boom knuckle crane [21] by the screw theory.

When large-size or slender payloads are transported, the crane systems often exhibit more complicated second-mode oscillations. In this situation, the single pendulum model is insufficient to capture the complex dynamics of the crane systems. Therefore, double pendulum models have been derived for various cranes, including modeling of a tower crane [22], modeling of an overhead crane [23]–[25], modeling of a boom crane [26], [27] by the Lagrangian method, and modeling of a bridge crane [28]–[30] using the Kane's method. To obtain a more accurate representation of the double pendulum cranes, some researchers took consideration of other factors' effect in their models. For the double-pendulum overhead crane, Jaafar and Mohamed derived the nonlinear dynamic model of it with constant hoisting cables [23]. For the transportation of a large object, the payload is generally connected to the hook by several rigging cables. As a result, the payload might twist about the rigging cables which makes the transportation task more challenging. Jie Huang built a linearized model of a double-pendulum overhead crane, with which he analyzed the two mode frequencies of payload swing and the variation in the frequency of the payload twisting [28], [29]. He further built a model of a double-pendulum bridge crane with wind gusts, taking the external wind disturbances into account [30].

During the offshore crane operations, sometimes extra passive/active mechanical system (e.g., Maryland Rigging [31]–[33] and Rider Block Tagline System [34], [35] is installed on the crane to suppress the payload swing to a reasonable range. In this scenario, the crane system can be defined as a constrained pendulum. Bing Wen derived a linearized model of shipboard crane with the Maryland Rigging by the Lagrangian method. Based on this model, numerical resonant frequencies of Maryland Rigging were calculated and verified with the complete nonlinear model [36]. Parker and Graziano presented an inverse kinematics control strategy for a crane equipped with Rider Block Tagline System (RBTS). Simulation results showed that a fixed inertial position of the payload can be held consuming 80% less power using RBTS compared to using the crane's actuations (slew, luff, and hoist) alone [35]. On the basis of Parker's research, Ku and Cha built a dynamic model of the multibody system by the Newton's equation, along which they employed a proportional-derivative controller to control the taglines' tensions [34]. However, the focus of Parker and Ku's work was on the control strategy of the taglines and the dynamics of the constrained pendulum system was largely ignored. Also, as the payload, the hoist cable, the main jib and the taglines always stay in a vertical plane, their dynamic model only considers the payload in-plane swing excited by the ship's pitch motion, which is insufficient for capturing the complex dynamics of the system.

In this paper, a novel Cable-Driven Inverted Tetrahedron Mechanism (CDITM) is proposed. Comparing to existing mechanical anti-swing methods like RBTS or Maryland Rigging, the main differences of the proposed method are as follows:

(1) The proposed structure forms an inverted tetrahedron in the space by three taglines, which can restrain the payload swing in any directions and does not reduce the crane's effective workspace.

(2) The taglines are connected to a redesigned hook, the frictional problem of the rider block in existing methods like RBTS is avoid and the service time of the hoist cable can be greatly prolonged.

(3) The hoist cable of the crane can be kept in vertical direction, the tensions of the taglines are mainly used to suppress the payload swing, thus the driven power of the tagline winches is minimized.

(4) the proposed mechanical structure has the advantages of high controllability, strong resistance to external excitation disturbance, simple structure and convenient installation.

The unique spatial configuration of CDITM enables it to suppress the payload swing in arbitrary directions. The main contribution of this paper is as follows:

(1) The three-dimensional kinematic and dynamic models of CDITM are built under the ship's roll and pitch excitations, which lay the theoretical foundation for position synchronization and payload swing suppression.

(2) To explore the complex dynamics of the constrained pendulum system with a moving base, the effect of ship excitations, tagline tensions, crane pose and the configuration of CDITM on the payload swing are thoroughly studied. The theoretical results might be very useful for structure optimization of CDITM and prediction of the payload swing during the design phase.

(3) Unlike most reported work related to dynamics of the offshore cranes where only numerical simulations are presented, we provide more convincing physical experiments. It is shown that the simulation patterns follow the experiment curves quite well, thus validating our theoretical work.

The novelty of this paper is reflected in two aspects:

(1) the novel structure of Cable-Driven Inverted Tetrahedron Mechanism (CDITM) is first proposed, it can restrain the payload swing in any directions and does not reduce the crane's effective workspace.

(2) the ship-crane-CDITM system is simplified as a constrained pendulum with base excitations, its three dimensional model is first built by the combined application of Newton-Euler method and robot kinematics.

This paper is outlined as follows. ''Structure of CDITM'' section briefly describes the structure of CDITM. ''Dynamic modelling of CDITM'' section builds the dynamic model of CDITM. ''Dynamic analysis'' section explores the effect of ship excitations, tagline tensions, crane pose and the configuration of CDITM on the payload swing. ''Experiment verifications'' section verifies the dynamic modeling and analysis of CDITM by physical experiments. Finally, the last section concludes this paper.

II. STRUCTURE OF CDITM

In a typical configuration of RBTS, two taglines are installed symmetrically on the left and right side of the main jib. Due to the nature of this configuration, the taglines are able to pull the payload, but they cannot push the payload away from the crane. In the previous physical experiments of RBTS, it was found that an inclined angle of the hoist cable was maintained. In this situation, the hoist cable acquires the capability to pull the payload away from the crane, allowing for suppression of payload motions in arbitrary directions. However, the trade-off is that a part of the payload weight might be carried by the taglines, meanwhile, the effective working space of the crane will be significantly reduced. Therefore, a novel Cable-Driven Inverted Tetrahedron Mechanism (CDITM) is proposed to overcome RBTS's side effects, as shown in Figure 1. As illustrated, the crane is composed of a hook, a hoist cable, a main jib and a crane housing. The CDITM contains three taglines, three anti-swing knuckle jibs and their driving system. Since the taglines form an inverted tetrahedron structure in the space, they are capable of suppressing the payload swing in any directions, meanwhile, the direction of the hoist cable can be kept as a vertical or near vertical state.

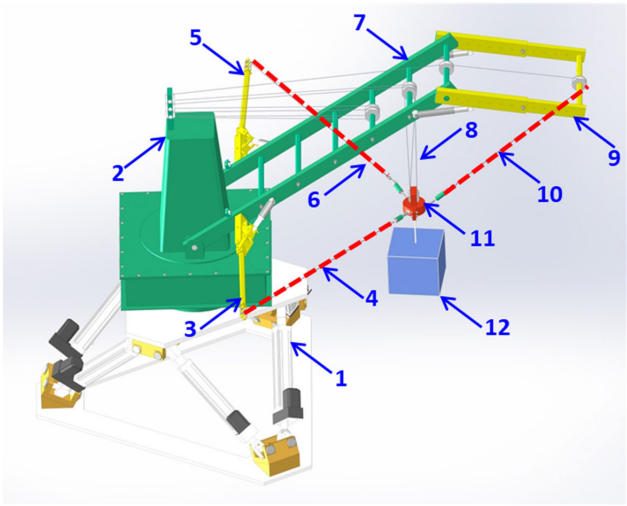

FIGURE 1. Three-dimensional diagram of the offshore crane with CDITM.

III. DYNAMIC MODELING OF CDITM

In the previous work of Ku *et al.* [34], the capacity of the motor was not considered in the mathematical model. Instead, they settle on a trial-and-error method for motor selection. In their experiments, they had to replace the 3 W DC motor by another 10 W DC motor with a larger maximum torque because the former could not control the payload swing to an acceptable range. Obviously, the trial-and-error method is less practical in engineering. Therefore, to guarantee the effectiveness of payload swing suppression in all possible conditions, it is quite necessary to build a three-dimensional dynamic model of the system which can be employed to analyze the minimum value of the taglines' tensions needed. Then the minimum power or torque of each motor can be selected in a more reasonable way based on the calculated minimum tension of the corresponding tagline.

The offshore crane with cable driven mechanism is a multiple-degree-of-freedom system (the ship has six degrees of freedom, the crane has three and the cable driven mechanism has three), it is difficult to build its three dimensional model using traditional method like Lagrangian method. To tackle the problem of three dimensional modeling of the ship-crane-CDITM system, it is simplified as a constrained pendulum with base excitations, its three dimensional model is first built by the combined application of Newton-Euler method and robot kinematics.

A. AKINEMATIC MODEL

Geometrically, Figure 1 is simplified and redrawn as Figure 2. As illustrated, $x_0y_0z_0$ is defined as the inertial frame, $x_1y_1z_1$ the ship based frame, $x_2y_2z_2$ the crane based frame. It is assumed that the hook is close enough to the payload, then they together can be lumped as a mass point, expressed as P. O_2E represents the main jib, PD the hoist cable; EF, HMN and HRS represents the anti-swing knuckle jib I, II, and III, respectively; PF, PN and PS represents the tagline I, II, and III, respectively. As seen in the top view, HMN and HRS are symmetrical about O_2E. Meanwhile, θ_{2y} is defined as the main jib's luff angle, θ_{2z} as the crane's slew angle; θ_{1x} and as θ_{1y} as the ship's pitch and roll angle, respectively; β_1 and β_2 as the luff angle of the anti-swing knuckle jib I and II, respectively; ψ_o and ψ_i as the out-plane and in-plane swing angle of the payload, respectively. Moreover, define ${}^0\mathbf{P}_P = [x_P\ y_P\ z_P]^T$ as the coordinates of P in $x_0y_0z_0$, L_{PN} as the spatial distance from N to P. Other expressions are obtained similarly.

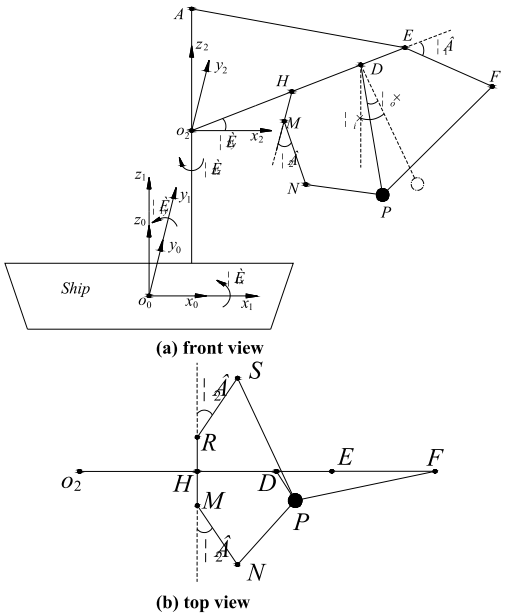

FIGURE 2. Simplified diagram of the offshore crane with CDITM.

As shown in Figure 2, it is easy to get the coordinates of P in $x_2y_2z_2$ by geometrical relations:

$$ {}^2\mathbf{P}_P = \begin{bmatrix} L_{O_2D}\cos\theta_{2y} + L_{PD}\cos\psi_o\sin\psi_i \\ -L_{PD}\sin\psi_o \\ L_{O_2D}\sin\theta_{2y} - L_{PD}\cos\psi_o\cos\psi_i \end{bmatrix} \tag{1} $$

Similarly, the expressions of ${}^0\mathbf{P}_D$, ${}^0\mathbf{P}_N$, ${}^0\mathbf{P}_S$ and ${}^0\mathbf{P}_F$ can be easily obtained.

Define $\mathbf{R}_x$, $\mathbf{R}_y$ and $\mathbf{R}_z$ as simple rotation matrix about x-axis, y-axis and z-axis respectively, and they are expressed as [37]:

$$ \begin{aligned} \mathbf{R}_x &= \begin{bmatrix} 1 & 0 & 0 \\ 0 & \cos\theta_x & \sin\theta_x \\ 0 & -\sin\theta_x & \cos\theta_x \end{bmatrix} \\ \mathbf{R}_y &= \begin{bmatrix} \cos\theta_y & 0 & -\sin\theta_y \\ 0 & 1 & 0 \\ \sin\theta_y & 0 & \cos\theta_y \end{bmatrix} \\ \mathbf{R}_z &= \begin{bmatrix} \cos\theta_z & \sin\theta_z & 0 \\ -\sin\theta_z & \cos\theta_z & 0 \\ 0 & 0 & 1 \end{bmatrix} \end{aligned} \tag{2} $$

Define ${}^m_n\mathbf{R}$ as the rotation matrix from $x_ny_nz_n$ to $x_my_mz_m$. The rotation matrixes from the inertial frame to the ship based frame and the crane based frame are:

$$ {}^1_0\mathbf{R} = \mathbf{R}_x(\theta_{1x})\mathbf{R}_y(\theta_{1y}) \tag{3} $$

$$ {}^2_0\mathbf{R} = \mathbf{R}_x(\theta_{1x})\mathbf{R}_y(\theta_{1y})\mathbf{R}_z(\theta_{2z}) \tag{4} $$

Then the payload position in the inertial frame is calculated by the following equation:

$$ {}^0\mathbf{P}_P = {}^0\mathbf{P}_1 + {}^1_0\mathbf{R}^{\mathrm{T}}{}^1\mathbf{P}_2 + {}^2_0\mathbf{R}^{\mathrm{T}}{}^2\mathbf{P}_P \tag{5} $$

where ${}^0\mathbf{P}_1 = [0 \quad 0 \quad 0]^{\mathrm{T}}$ is the coordinates O_1 in $x_0y_0z_0$, ${}^1\mathbf{P}_2 = [L_x \quad L_y \quad L_z]^{\mathrm{T}}$is the coordinates O_2 in $x_1y_1z_1$.

Substitute (1), (3) and (4) into (5), the expressions of x_P, y_P, and z_P are obtained:

$$ \begin{aligned} x_P = {} & L_x\cos\theta_{1y} + \cos\theta_{2z}\left(L_{PD}\cos\psi_o\sin\psi_i + L_{O_2D}\cos\theta_{2y}\right) \\ & \times \cos\theta_{1y} + L_z\cos\theta_{1x}\sin\theta_{1y} + L_y\sin\theta_{1x}\sin\theta_{1y} \\ & + L_{PD}\sin\psi_o\left(\cos\theta_{1x}\sin\theta_{2z} - \cos\theta_{2z}\sin\theta_{1x}\sin\theta_{1y}\right) \\ & + \left(L_{O_2D}\sin\theta_{2y} - L_{PD}\cos\psi_i\cos\psi_o\right)\left(\cos\theta_{1x}\cos\theta_{2z}\sin\theta_{1y}\right. \\ & \left. + \sin\theta_{1x}\sin\theta_{2z}\right) \end{aligned} \tag{6} $$

$$ \begin{aligned} y_P = {} & \cos\theta_{1y}\left(L_{PD}\cos\psi_o\sin\psi_i + \cos\theta_{2y}L_{O_2D}\right)\sin\theta_{2z} \\ & - L_{PD}\sin\psi_o\left(\cos\theta_{1x}\cos\theta_{2z} + \sin\theta_{1x}\sin\theta_{1y}\sin\theta_{2z}\right) \\ & + \left(L_{PD}\cos\psi_i\cos\psi_o - L_{O_2D}\sin\theta_{2y}\right)\left(\cos\theta_{2z}\sin\theta_{1x}\right. \\ & \left. - \cos\theta_{1x}\sin\theta_{1y}\sin\theta_{2z}\right) + L_y\cos\theta_{1x} - L_z\sin\theta_{1x} \end{aligned} \tag{7} $$

$$ \begin{aligned} z_P = {} & \cos\theta_{1x}\cos\theta_{1y}\left(-L_{PD}\cos\psi_i\cos\psi_o + L_z + L_{O_2D}\sin\theta_{2y}\right) \\ & - \left(L_x + L_{PD}\cos\psi_o\sin\psi_i + L_{O_2D}\cos\theta_{2y}\right)\sin\theta_{1y} \\ & + \left(L_y - L_{PD}\sin\psi_o\right)\cos\theta_{1y}\sin\theta_{1x} \end{aligned} \tag{8} $$

Similarly, the coordinates of D, N, S and F in $x_0y_0z_0$ can be obtained as well.

Assume the taglines are always in tension, then the length of tagline I is the distance from P to F:

$$ L_{PF} = \sqrt{(x_F - x_P)^2 + (y_F - y_P)^2 + (z_F - z_P)^2} \tag{9} $$

Meanwhile, the expressions of the length of tagline II and III can be obtained in the same way. Note that these expressions do not apply to the scenario when the taglines are slack. When the tagline becomes slack, the tension of it decreases to nearly 0 and the shape of it is a catenary. In such a state, the tagline might jump out of the winch drum or the guiding pulley, so the pre-tensioning mechanism or control method is always needed in practice to avoid such problem. Also, this implies the tagline tension must always be positive in the simulation model. $\dot{\theta}_{2z} = 0$.

Assume $\dot{\theta}_{2z} = 0$, $\dot{\theta}_{2y} = 0$, take second derivative of the coordinates of D, the acceleration of D in $x_0y_0z_0$ is (10)–(12), as shown at the bottom of the next page.

As shown in Figure 2, the geometrical relations between P and D is:

$$ {}^0\mathbf{P}_P = {}^0\mathbf{P}_D + \begin{bmatrix} L_{PD}\cos\psi_o\sin\psi_i \\ -L_{PD}\sin\psi_o \\ -L_{PD}\cos\psi_o\cos\psi_i \end{bmatrix} \tag{13} $$

Then take second derivative of (13), the acceleration of P, $\mathbf{a}_P$, in $x_0y_0z_0$ is:

$$ \begin{aligned} \ddot{x}_P = {} & \ddot{x}_D + L_{PD}\cos\psi_i\left(\ddot{\psi}_i\cos\psi_o - 2\dot{\psi}_i\dot{\psi}_o\sin\psi_o\right) \\ & - L_{PD}\sin\psi_i\left(\cos\psi_o\left(\dot{\psi}_i^2 + \dot{\psi}_o^2\right) + \ddot{\psi}_o\sin\psi_o\right) \end{aligned} \tag{14} $$

$$ \ddot{y}_P = \ddot{y}_D + L_{PD}\dot{\psi}_o^2\sin\psi_o - L_{PD}\ddot{\psi}_o\cos\psi_o \tag{15} $$

$$ \ddot{z}_P = \ddot{z}_D + L_{PD}\begin{pmatrix} \cos\psi_i\cos\psi_o\dot{\psi}_i^2 - 2\dot{\psi}_o\dot{\psi}_i\sin\psi_i\sin\psi_o \\ +\cos\psi_i\cos\psi_o\dot{\psi}_o^2 + \ddot{\psi}_i\cos\psi_o\sin\psi_i \\ +\ddot{\psi}_o\cos\psi_i\sin\psi_o \end{pmatrix} \tag{16} $$

B. DYNAMIC MODEL

In the inertial frame, the payload can be isolated and the forces exert on it are shown as Figure 3. As illustrated, $\mathbf{F_1}$,

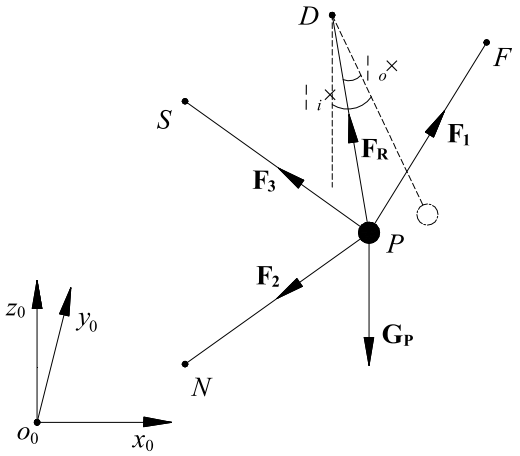

FIGURE 3. Free body diagram of the payload.

$\mathbf{F_2}$ and $\mathbf{F_3}$ represents the tension of tagline I, II, and III, respectively; $\mathbf{G_P}$ the payload gravity; $\mathbf{F_R}$ the tension of the hoist cable.

Define $\mathbf{G_P} = [0\ 0\ m_P g]^{\mathrm{T}}$, $\mathbf{F_R} = [F_{Rx}\ F_{Ry} F_{Rz}]^{\mathrm{T}}$, $\mathbf{F_1} = [F_{1x} F_{1y}\ F_{1z}]^{\mathrm{T}}$, $\mathbf{F_2} = [F_{2x} F_{2y}\ F_{2z}]^{\mathrm{T}}$, $\mathbf{F_3} = [F_{3x} F_{3y}\ F_{3z}]^{\mathrm{T}}$, where g is the acceleration of gravity and m_P is the mass of the payload and. Define the force components of $\mathbf{F_1}$ along x_0, y_0 and z_0 axis as:

$$\left[F_{1x}\ F_{1y}\ F_{1z} \right]^{\mathrm{T}} = \left[|\mathbf{F_1}|\, i_{1x}\ |\mathbf{F_1}|\, i_{1y}\ |\mathbf{F_1}|\, i_{1z} \right]^{\mathrm{T}} \tag{17}$$

where $|\mathbf{F_1}|$ is the magnitude of vector $\mathbf{F_1}$, $i_{1x} = (x_F - x_P)/L_{PF}$, $i_{1y} = (y_F - y_P)/L_{PF}$, $i_{1z} = (z_F - z_P)/L_{PF}$. Similarly, the force components of $\mathbf{F_2}$ and $\mathbf{F_3}$ can be obtained.

The force components of $\mathbf{F_R}$ along x_0, y_0 and z_0 axis are:

$$\begin{cases} F_{Rx} = -|\mathbf{F_R}| \cos\psi_o \sin\psi_i \\ F_{Ry} = |\mathbf{F_R}| \sin\psi_o \\ F_{Rz} = |\mathbf{F_R}| \cos\psi_o \cos\psi_i \end{cases} \tag{18}$$

Then the equation of motion for the payload can be obtained based on Newton's second Law:

$$m\mathbf{a}_P = \mathbf{F}_1 + \mathbf{F}_2 + \mathbf{F}_3 + \mathbf{F}_R - \mathbf{G}_P \tag{19}$$

Finally, substitute (14)-(18) into (19), the equations of motion for the constrained pendulum system are obtained by proper simplification:

$$\ddot{\psi}_i = \left(\sec\psi_o \begin{pmatrix} \cos\psi_i \left(f_x - m\ddot{x}_D\right) + \\ \sin\psi_i \left(f_z - m\left(\ddot{z}_D + g\right)\right) + \\ 2L_{PD} m \dot{\psi}_i \dot{\psi}_o \sin\psi_o \end{pmatrix} \right) / \left(L_{PD} m\right) \tag{20}$$

$$\ddot{\psi}_o = \begin{pmatrix} \sin\psi_i \sin\psi_o \left(m\ddot{x}_D - f_x\right) - \\ \cos\psi_o \left(-m\ddot{y}_D + f_y + L_{PD} m \dot{\psi}_i^2 \sin\psi_o\right) \\ + \cos\psi_i \sin\psi_o \left(f_z - m\left(\ddot{z}_D + g\right)\right) \end{pmatrix} / \left(L_{PD} m\right) \tag{21}$$

where $f_x = F_{1x} + F_{2x} + F_{3x}$, $f_y = F_{1y} + F_{2y} + F_{3y}$ and $f_z = F_{1z} + F_{2z} + F_{3z}$ is the resultant force of the taglines along x_0, y_0 and z_0 axis, respectively.

When the inertial and delay of tagline's driving system is considered, the winch dynamics can be formulated as:

$$J_i \ddot{q}_i + c_i \dot{q}_i + r\,|F_i| = \tau_i \qquad i = 1, 2, 3 \tag{22}$$

where J_i is the inertia of the winch, c_i denotes the coefficient for winch viscous friction, r is radius of the winch, τ_i is the torque generated by the winch, $|F_i|$ is the tagline tension which is given by:

$$|F_i| = k_i \left(r\Delta q_i + \Delta L_{id} + \Delta L_{is}\right) \qquad i = 1, 2, 3 \tag{23}$$

where k_i is stiffness coefficient of the tagline, Δq_i represents the rotation angle of the winch, ΔL_{id} denotes the tagline elongation caused by payload motion, ΔL_{is} is the inertial elongation caused by pre-tensioning force of the tagline.

IV. DYNAMIC ANALYSIS

As a common physical phenomenon, the freely swing of the payload might finally come to rest no matter how long it takes because of the air damping. Inspired by this phenomenon, a setting method of tagline tension is presented in order to ensure that the payload swing would always be damped by

$$\begin{aligned} \ddot{x}_D = {} & \ddot{\theta}_{1y} \left(L_y \cos\theta_{1y} \sin\theta_{1x} - \left(L_x + L_{O_2D} \cos\theta_{2y} \cos\theta_{2z}\right) \sin\theta_{1y} + \cos\theta_{1x} \cos\theta_{1y} \left(L_z + L_{O_2D} \cos\theta_{2z} \sin\theta_{2y}\right)\right) \\ & + \dot{\theta}_{1y} \begin{pmatrix} \cos\theta_{1y} \dot{\theta}_{1x} \left(L_y \cos\theta_{1x} - \sin\theta_{1x} \left(L_z + L_{O_2D} \cos\theta_{2z} \sin\theta_{2y}\right)\right) \\ -\dot{\theta}_{1y} \begin{pmatrix} \cos\theta_{1y} \left(L_x + L_{O_2D} \cos\theta_{2y} \cos\theta_{2z}\right) \\ + \sin\theta_{1y} \left(L_y \sin\theta_{1x} + \cos\theta_{1x} \left(L_z + L_{O_2D} \cos\theta_{2z} \sin\theta_{2y}\right)\right) \end{pmatrix} \end{pmatrix} \\ & + \ddot{\theta}_{1x} \left(\cos\theta_{1x} \left(L_y \sin\theta_{1y} + L_{O_2D} \sin\theta_{2y} \sin\theta_{2z}\right) - \sin\theta_{1x} \sin\theta_{1y} \left(L_z + L_{O_2D} \cos\theta_{2z} \sin\theta_{2y}\right)\right) \\ & + \dot{\theta}_{1x} \begin{pmatrix} \cos\theta_{1y} \dot{\theta}_{1y} \left(L_y \cos\theta_{1x} - \sin\theta_{1x} \left(L_z + L_{O_2D} \cos\theta_{2z} \sin\theta_{2y}\right)\right) \\ -\dot{\theta}_{1x} \begin{pmatrix} \cos\theta_{1x} \sin\theta_{1y} \left(L_z + L_{O_2D} \cos\theta_{2z} \sin\theta_{2y}\right) \\ + \sin\theta_{1x} \left(L_y \sin\theta_{1y} + L_{O_2D} \sin\theta_{2y} \sin\theta_{2z}\right) \end{pmatrix} \end{pmatrix} \end{aligned} \tag{10}$$

$$\begin{aligned} \ddot{y}_D = {} & \left(\sin\theta_{1x} \left(L_z + L_{O_2D} \cos\theta_{2z} \sin\theta_{2y}\right) - \cos\theta_{1x} \left(L_y + L_{O_2D} \sin\theta_{1y} \sin\theta_{2y} \sin\theta_{2z}\right)\right) \dot{\theta}_{1x}^2 \\ & - L_{O_2D} \left(\left(\cos\theta_{1y} \cos\theta_{2y} + \cos\theta_{1x} \sin\theta_{1y} \sin\theta_{2y}\right) \dot{\theta}_{1y}^2 + \ddot{\theta}_{1y} \left(\cos\theta_{2y} \sin\theta_{1y} - \cos\theta_{1x} \cos\theta_{1y} \sin\theta_{2y}\right)\right) \sin\theta_{2z} \\ & - \ddot{\theta}_{1x} \left(\cos\theta_{1x} \left(L_z + L_{O_2D} \cos\theta_{2z} \sin\theta_{2y}\right) + \sin\theta_{1x} \left(L_y + L_{O_2D} \sin\theta_{1y} \sin\theta_{2y} \sin\theta_{2z}\right)\right) \\ & - 2\dot{\theta}_{1y} \dot{\theta}_{1x} L_{O_2D} \cos\theta_{1y} \sin\theta_{1x} \sin\theta_{2y} \sin\theta_{2z} \end{aligned} \tag{11}$$

$$\begin{aligned} \ddot{z}_D = {} & \dot{\theta}_{1y} \dot{\theta}_{1x} \sin\theta_{1y} \left(\sin\theta_{1x} \left(L_z + L_{O_2D} \sin\theta_{2y}\right) - L_y \cos\theta_{1x}\right) - \dot{\theta}_{1x}^2 \cos\theta_{1y} \left(L_y \sin\theta_{1x} + \cos\theta_{1x} \left(L_z + L_{O_2D} \sin\theta_{2y}\right)\right) \\ & + \ddot{\theta}_{1x} \cos\theta_{1y} \left(L_y \cos\theta_{1x} - \sin\theta_{1x} \left(L_z + L_{O_2D} \sin\theta_{2y}\right)\right) \\ & - \ddot{\theta}_{1y} \left(\cos\theta_{1y} \left(L_x + L_{O_2D} \cos\theta_{2y}\right) + \sin\theta_{1y} \left(L_y \sin\theta_{1x} + \cos\theta_{1x} \left(L_z + L_{O_2D} \sin\theta_{2y}\right)\right)\right) \\ & - \dot{\theta}_{1y} \begin{pmatrix} \dot{\theta}_{1y} \left(L_y \cos\theta_{1y} \sin\theta_{1x} - \left(L_x + L_{O_2D} \cos\theta_{2y}\right) \sin\theta_{1y} + \cos\theta_{1x} \cos\theta_{1y} \left(L_z + L_{O_2D} \sin\theta_{2y}\right)\right) \\ + \dot{\theta}_{1x} \sin\theta_{1y} \left(L_y \cos\theta_{1x} - \sin\theta_{1x} \left(L_z + L_{O_2D} \sin\theta_{2y}\right)\right) \end{pmatrix} \end{aligned} \tag{12}$$

the taglines' resultant force, as follows:

$$\begin{cases} F_{1s} - \delta_1 \le |\mathbf{F_1}| \le F_{1s} + \delta_1 \\ F_{2s} - \delta_2 \le |\mathbf{F_2}| \le F_{2s} + \delta_2 \\ F_{3s} - \delta_3 \le |\mathbf{F_3}| \le F_{3s} + \delta_3 \end{cases} \tag{24}$$

where F_{1s}, F_{2s} and F_{3s} are the static pre-tensioning tensions which are satisfied with the static equilibrium condition; δ_1, δ_2 and δ_3 are the tensions' thresholds.

The effectiveness of the aforementioned tagline tension setting method has been validated in physical experiments. However, the system behaviors under ship excitations and parametric variations of the system still remain unknown and might be quite complex. Therefore, to explore the complex dynamics of the constrained pendulum system, the influence law of ship excitations, tagline tensions, crane pose and CDITM configuration on the payload swing will be studied thoroughly. The default system parameters are shown in Table 1, which are consistent with the physical experimental setup. On the basis of the dynamic models built in Section 3, the dynamic analysis will be carried out by numerical simulations using Matlab/Simulink.

TABLE 1. The default system parameters.

Parameters	value	Parameters	value
L_{PD}	1.20 m	θ_{1x}	0
L_{OD}	1.20 m	θ_{1y}	6sin(πt/3)
L_{OE}	1.20 m	θ_{2y}	45°
L_{EF}	0.50 m	θ_{2z}	0°
L_{OH}	0.32 m	m_P	25 kg
L_{HM}	0.25 m	g	9.8 m/s^2
L_{MN}	0.75 m	F_{1s}	40 N
L_x	0 m	F_{2s}	10.92 N
L_y	0 m	F_{3s}	10.92 N
L_z	0.42 m	δ_1	11 N
β_1	0°	δ_2	3 N
β_2	10°	δ_3	3 N

A. EFFECT OF SHIP EXCITATIONS

By varying the amplitude of ship roll motion from 4° to 8°, the payload swing under different ship roll excitations are obtained, demonstrated in Figure 4. As illustrated, the in-plane swing tends to increase with the increasing ship roll amplitude, while the out-plane swing remains 0 which indicates that ship roll motion can only excite the payload in-plane swing. Given ship roll amplitude as 0 and ship pitch amplitude as 4° to 8°, the effect of ship pitch on the payload swing is depicted as Figure 5. Surprisingly, both the out-plane swing and the in-plane swing are excited, and they have the tendency to increase as the ship pitch amplitude increases. Referring to Figure 2, the reason why the in-plane swing is excited by the ship pitch motion can be explained as follows: when the out-plane is excited by the ship pitch motion, the tagline I is not in the vertical plane with the main jib O_2E, then the tension of tagline I has an in-plane component and an out-plane component, as a result, the in-plane component acts as an excitation for the in-plane swing.

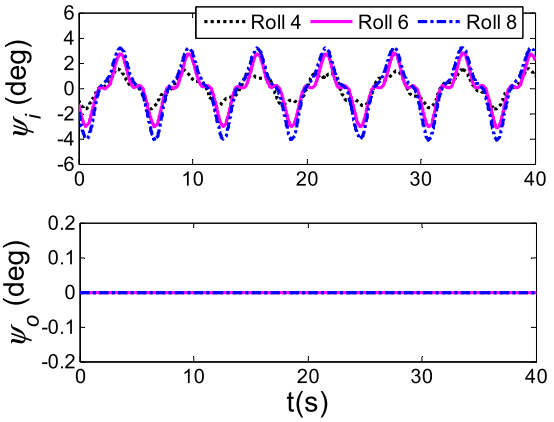

FIGURE 4. Effect of ship roll on the payload swing.

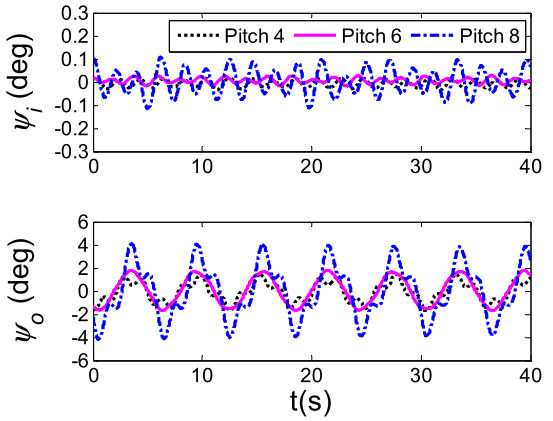

FIGURE 5. Effect of ship pitch on the payload swing.

B. EFFECT OF TAGLINE TENSIONS

As mentioned above, equation (22) is used for tagline tension setting which can ensure that the payload swing would always be damped by the taglines' resultant force. In this subsection, effect of the static tagline tensions (F_{1s}, F_{2s} and F_{3s}) and the tension thresholds (δ_1, δ_2 and δ_3) on the payload swing suppression will be investigated. Given $\delta_1 = 11$ N, $\delta_2 = \delta_3 = 3$ N, the payload swing can be obtained for $F_{1s} = 25$ to 54 N (F_{2s} and F_{3s} can be gotten by solving static equilibrium equation), shown as Figure 6. However, it is observed that the payload in-plane swing increases with the increasing of F_{1s}, in another word, the payload swing suppression becomes worse with the increasing of F_{1s}. Next, given $F_{1s} = 40$ N, $F_{2s} = F_{3s} = 10.92$ N, the payload swing can be obtained for $\delta_1 = 8$ to 24 N (δ_2 and δ_3 can be obtained by solving static equilibrium equation), shown as Figure 7. It is observed that the payload swing suppression gets better with bigger value of δ_1. Therefore, it can be concluded that the payload swing suppression gets better with smaller F_{1s} and larger δ_1.

C. EFFECT OF CRANE POSE

From Figure 1, it can be seen that the anti-swing knuckle jibs are mounted on the main jib of the crane. Due to this

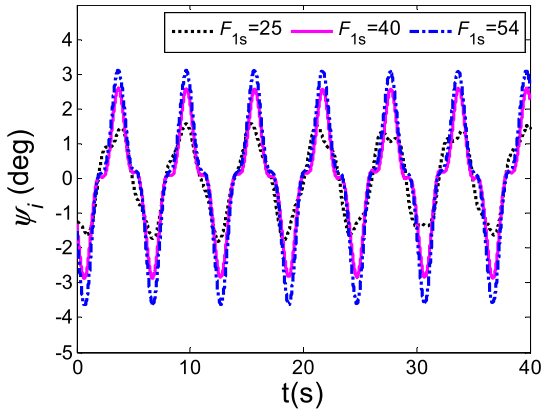

FIGURE 6. Effect of F_{1s} on the payload swing.

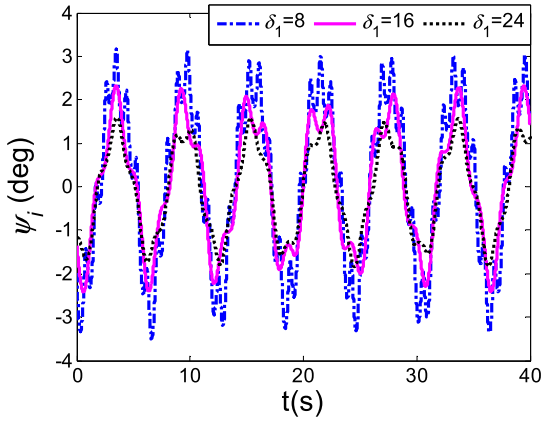

FIGURE 7. Effect of δ_1 on the payload swing.

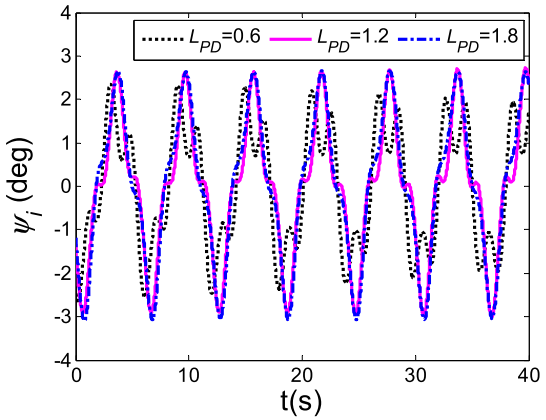

FIGURE 8. Effect of L_{PD} on the payload swing.

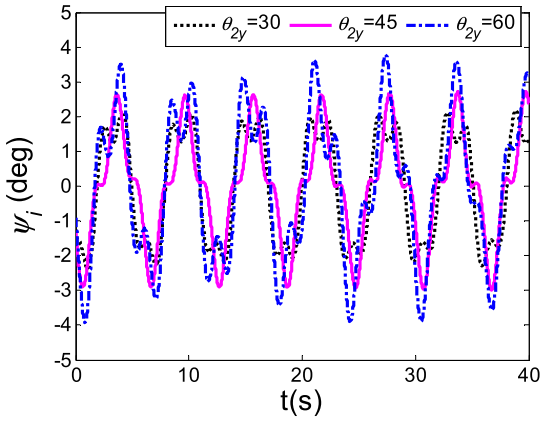

FIGURE 9. Effect of θ_{2y} on the payload swing.

architecture, the length of the hoist cable L_{PD} and the luff angle of the main jib θ_{2y} have great influence on the directions of the taglines, which causes further impact on the effect of payload swing suppression. Given $\theta_{2y} = 45°$, $\delta_1 = 24$ N, $\delta_2 = \delta_3 = 6.57$ N, and $L_{PD} = 0.6$ to 1.8 m, the effect of L_{PD} on the payload in-plane swing can be analyzed, shown as Figure 8. It is observed that the payload in-plane swing tends to increase when the hoist cable gets longer. Next, given $L_{PD} = 1.2$, $\delta_1 = 24$ N, $\delta_2 = \delta_3 = 6.57$ N, and $\theta_{2y} = 30°$ to 60°, the effect of θ_{2y} on the payload in-plane swing can be obtained, shown as Figure 9. The payload in-plane swing increases with the increasing of luff angle. As a result, it can be concluded that the payload swing suppression deteriorates with the increment in L_{PD} and θ_{2y}.

D. EFFECT OF CDITM CONFIGURATION

Except the crane pose, the directions of the taglines can be influenced by the configuration of CDITM as well. To get better effectiveness of payload swing suppression, the configuration of CDITM is a crucial factor and need to be optimized in a reasonable manner. In this subsection, the effect of some key parameters of CDITM configuration on the payload swing suppression will be studied.

Given $\delta_1 = 24$ N, $\delta_2 = \delta_3 = 6.57$ N, simulations are carried out for $\beta_1 = 0$ to 120°; for each case, the maximum value and variation range of the in-plane swing are analyzed and recorded, shown as Figure 10. The variation range is defined as the difference between the maximum and minimum value of payload swing. It can be noticed that they tend to decrease first and then increase. The minimum value of them are obtained when $\beta_1 = 60°$. Similarly, given $\delta_1 = 24$ N, $\delta_2 = \delta_3 = 6.57$ N, the maximum value and variation range of the in-plane swing are analyzed and recorded for $L_{EF} = 0.25$ to 2 m. It is observed that they keep the overall tendency to decrease with the increasing L_{EF}. To conclude, the effect of payload swing suppression gets better with the increasing L_{EF}, while it gets better first and then gets worth with the increasing β_1.

Given $\delta_1 = 24$ N, $\delta_2 = \delta_3 = 6.57$ N, $\theta_{1x} = 0$, and $\theta_{1y} = 6\sin(\pi t/3)$, simulations are carried out for $\beta_2 = 0$ to 80°, the maximum value and variation range of the in-plane swing are obtained, shown as Figure 12. It is obvious that both of them increase with the increasing of β_2. Similar results can be obtained when the system is excited by the ship pitch motion, i.e. $\theta_{1x} = 6\sin(\pi t/3)$, and $\theta_{1y} = 0$, shown as Figure 13. Therefore, it can be concluded that the payload swing suppression gets worse with the increasing of β_2.

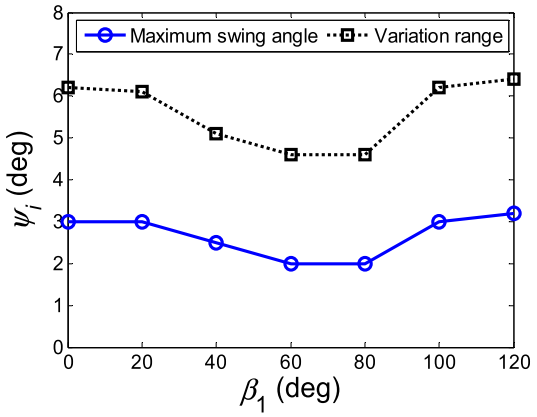

FIGURE 10. Effect of β_1 on the payload swing.

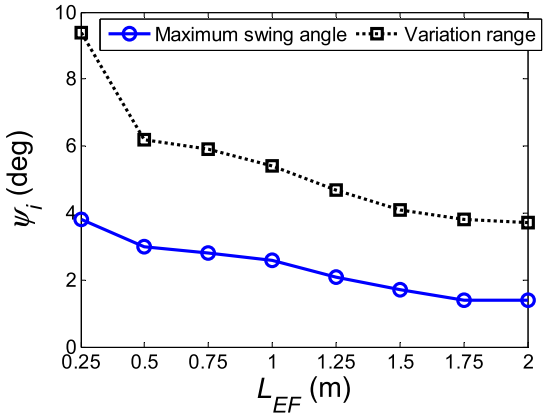

FIGURE 11. Effect of L_{EF} on the payload swing.

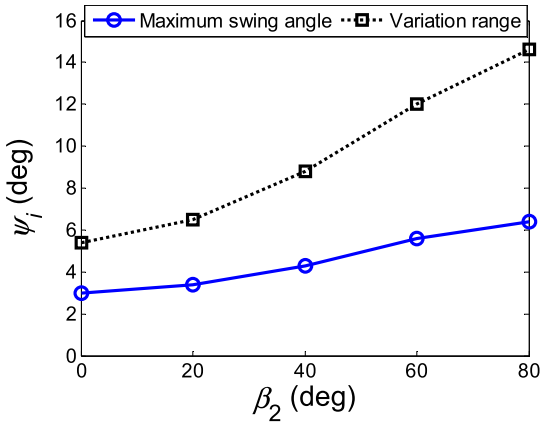

FIGURE 12. Effect of β_2 on the in-plane swing.

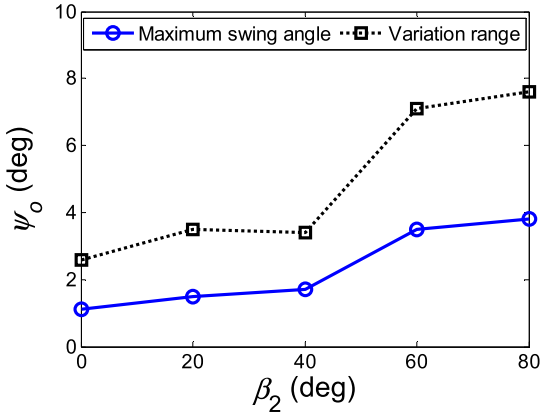

FIGURE 13. Effect of β_2 on the out-plane swing.

The effect of L_{MN} on the payload swing suppression is studied in the same way as β_2, simulations are carried out in two groups: (1) ship roll excitation case, i.e. $\theta_{1x} = 0$, and $\theta_{1y} = 6\sin(\pi t/3)$; (2) ship pitch excitation case, $\theta_{1x} = 6\sin(\pi t/3)$, and $\theta_{1y} = 0$. The results of these cases are illustrated as Figure 14 and Figure 15. The maximum value and variation range of the in-plane swing tend to increase when L_{MN} is less than 1.5, opposite tendencies are obtained for the out-plane swing; however, when L_{MN} is greater than 1.5, the in-plane swing tends to decrease at first and then increase, while the out-plane swing has the overall tendency to increase. Therefore, it can be concluded that when L_{MN} is less than 1.5, the in-plane swing suppression gets worse while the out-plane swing suppression gets better with the increasing L_{MN}.

V. EXPERIMENT VERIFICATIONS

A physical experiment platform of an offshore crane with CDITM is built in the Marine Hydraulic Crane Lab in Dalian Maritime University, shown as Figure 16.

It is mainly composed of mechanical structure, hydraulic drive system and control system. A novel Cable-Driven Inverted Tetrahedron Mechanism (CDITM) is located on the mechanical structure, and the cable is used to restrain the irregular swing of the payload; the hydraulic drive system receives the signal from the control system and provides driving force for the cable in the mechanical structure; the control system receives the cable tension feedback signal from the mechanical structure and the pressure feedback signal from the hydraulic drive system, and it sends control command to drive the tagline winch according to these signals.

In the physical experiment, since reversing valve and proportional valve are combined to control the rotation direction and speed of the tagline winch, it is difficult to avoid the hydraulic shock induced by the frequently action of the reversing valve. To avoid the hydraulic shock induced by the frequently action of the reversing valve, a damping based tagline tension setting method is proposed as equation (24) in the manuscript, the action frequency of the reversing valve can be significantly reduced by tuning the parameters of the tensions' thresholds.

The parameters of the experiment platform are consistent with the simulation listed in Table 1.

To verify the theoretical work in Section 3 and 4, experiment verifications are carried out for different ship roll excitations, i.e. $\theta_{1y} = 8\sin(\pi t/3)$ and $\theta_{1y} = 4\sin(\pi t/3)$. The experiment and simulation results are shown from Figure 17 to 20. It is shown that the simulation tendencies of in-plane swing follows the experiment curves quite well.

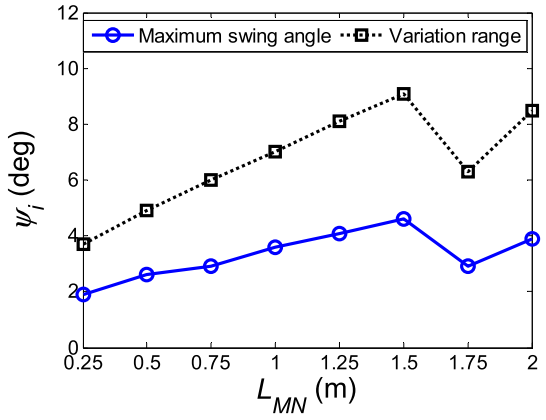

FIGURE 14. Effect of L_{MN} on the in-plane swing.

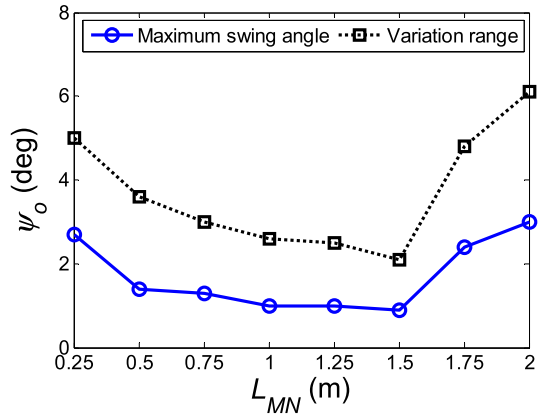

FIGURE 15. Effect of L_{MN} on the out-plane swing.

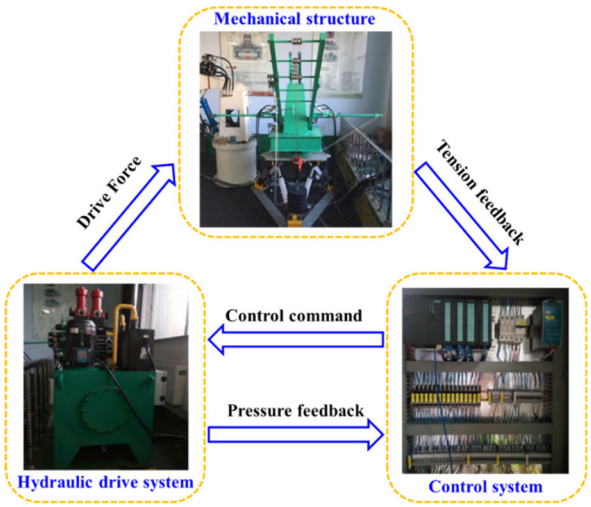

FIGURE 16. The physical experiment platform of an offshore crane with CDITM.

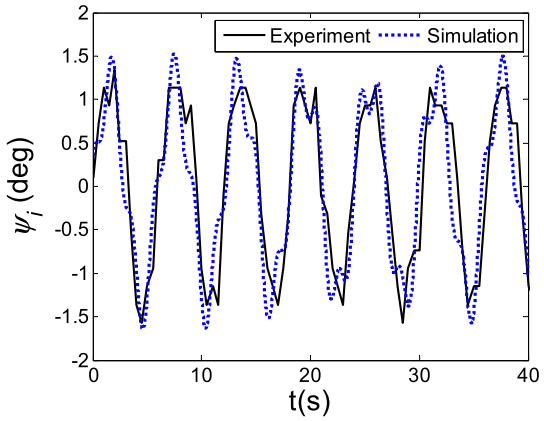

FIGURE 17. In-plane swing (ship roll 4 deg).

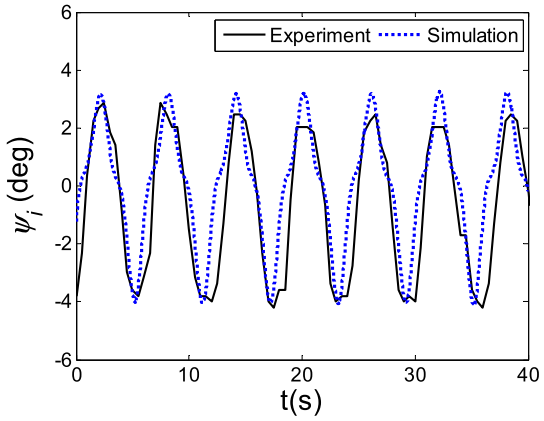

FIGURE 18. In-plane swing (ship roll 8 deg).

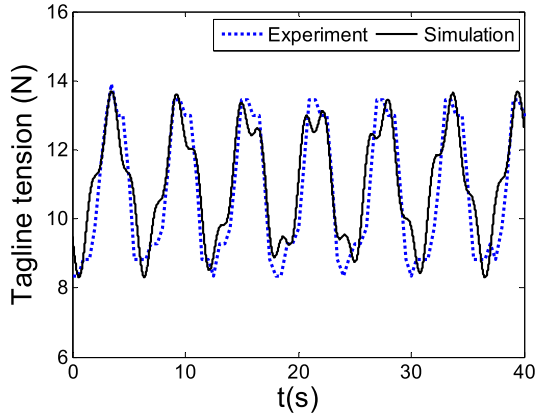

FIGURE 19. Tension of tagline II (ship roll 4 deg).

It can be calculated that the average deviation between the experiment and simulation results is 1.72° and 0.32° for $\theta_{1y} = 8\sin(\pi t/3)$ and $\theta_{1y} = 4\sin(\pi t/3)$, respectively. For these cases, the ratio of the average deviation with respect to the experimental deviation range is 24.2% and 10.9%, respectively. Meanwhile, it is noted that the simulation results of the tension of tagline II can be maintained in the setting range 7.94-13.94 N according to equation (22), but there is overshoot for the tension of tagline II in the experiment. This makes sense considering the following factors in physical experiment setup: (1) the delay and inertia of the driving system are difficult to calculate accurately; (2) the frequency

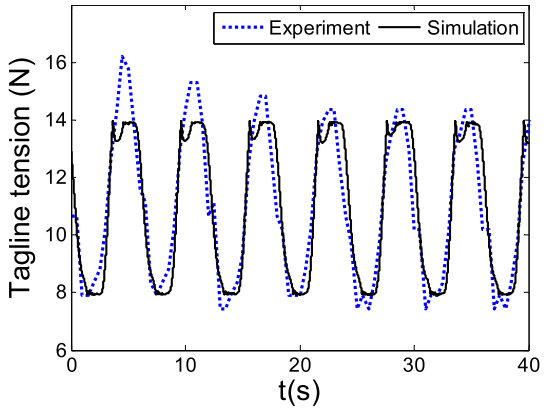

FIGURE 20. Tension of tagline II (ship roll 8 deg).

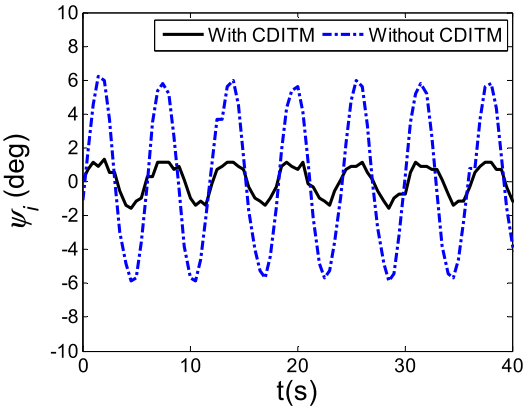

FIGURE 21. In-plane swing (with VS without CDTM, ship roll 4 deg).

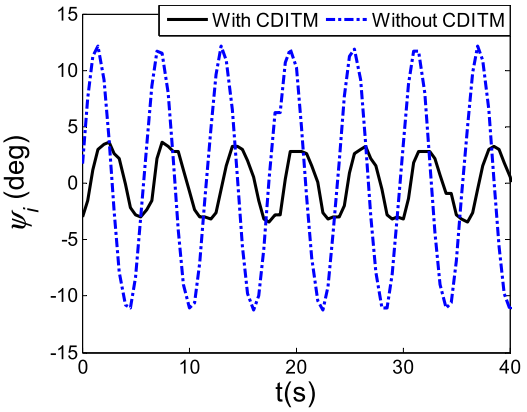

FIGURE 22. In-plane swing (with VS without CDTM, ship roll 8 deg).

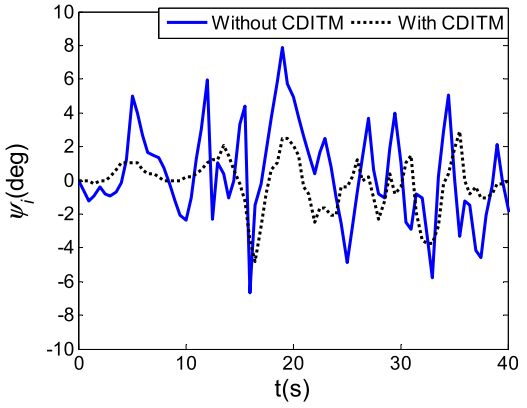

FIGURE 23. In-plane swing (with VS without CDTM, sea state 4).

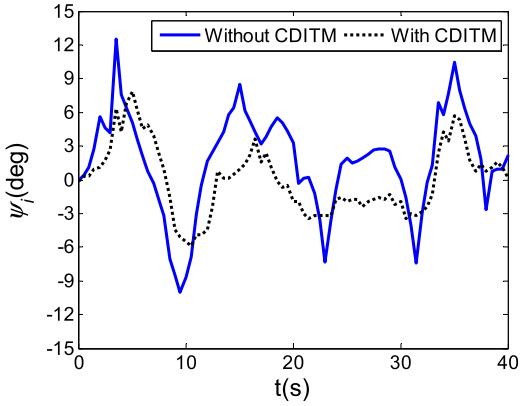

FIGURE 24. In-plane swing (with VS without CDTM, sea state 6).

of command signal is much lower in the experiment than that in the simulation; (3) the measuring error of payload swing might be induced by the high frequency vibration of the system; (4) the fit clearance of the anti-swing knuckle jib might affect the tension control precision of the tagline; (5) the compressibility of hydraulic pipeline is difficult to be modeled and is ignored in the simulation; (6) the influence of structure vibration on the payload swing is difficult to be modeled and is ignored in the simulation. In general, the simulation pattern of in-plane swing follows the experiment curves quite well, and the variations between the experiment and simulation results are acceptable. It can be concluded that the dynamic model built in Section 3 are verified, and the dynamic analysis in Section 4 are reasonable.

In order to verify the anti-swing performance of CDITM, the experimental platform in Figure 16 is used to carry out the comparative study under regular excitation. In the comparative experiments, the ship excitation is chosen as sinusoidal with amplitude 4 ° and 8 °, and the results are shown in Figure 21 and 22. From these figures, it can be seen that under the regular excitation, the period of the payload swing increases after the CDITM is installed, and the maximum positive and negative swing angles of the payload can be reduced by more than 76%. In other words, after using CDITM, it is found that the swing angle of the payload is relatively stable and the fluctuation range is small, which achieves the expected purpose.

Since the ship motion is not completely excited by regular environment excitation (sine function or cosine function of wave disturbance) in reality, it is necessary to consider the influence of irregular ship motion under nonlinear environment excitation. Then the universal effectiveness of anti-swing of the proposed method can be verified. Therefore,

the comparative experiments under irregular ship motion are carried out to test the effective range of CDITM.

The irregular ship motions under sea state 4 and 6 are generated using ship motion equation and nonlinear wave model. The experimental platform in Figure 16 is used to carry out the comparative study under nonlinear excitation, and the results are shown as Figure 23 and Figure 24 respectively. Without CDITM, the in-plane angle of the payload changes rapidly under the nonlinear ship excitation. After the CDITM is installed in sea state 4, the swing of the payload becomes smooth, and the instantaneous peak phenomenon of the in-plane angle of the payload is avoided. In sea state 6, it is noted that the swing period of payload increases after the CDITM is installed. From Figure 23 and 24, it is obvious the payload swing is relatively more stable with less fluctuation after the CDITM is installed, which verifies the effectiveness of the proposed method under nonlinear environment excitation.

Moreover, it is found that the effect of swing suppression of the CDITM in high sea state conditions is not as good as that in low sea state conditions. This is mainly due to the increased vibration of the offshore crane platform caused by high sea state conditions, which increases the uncertainty of the payload space motion and the difficulty of swing suppression of the payload.

VI. CONCLUSION

In this paper, the novel structure of CDITM for payload swing suppression in any directions is proposed. Further, the three-dimensional dynamic modelling of the system is carried out, with the equations of motion of the constrained pendulum with a moving base obtained. Next, to explore the complex dynamics of the constrained pendulum system, the effect of ship excitations, tagline tensions, crane pose and CDITM configuration on the payload swing are analyzed thoroughly. Finally, experiment verifications are conducted in a comparative manner. Through theoretical study and physical experiments, the following results are obtained:

(1) The payload swing suppression gets worse with the increasing of the ship excitations, the static tensions of the taglines, the hoist cable length, the luff angle of the main jib or the luff angle of the anti-swing knuckle jib II. On the contrary, it gets better with the increasing of the thresholds of the tensions or the length of anti-swing knuckle jib I.

(2) With the increasing luff angle of the anti-swing knuckle jib I, the payload swing suppression gets better first and worsens later. Meanwhile, when the length of anti-swing knuckle jib II is less than 1.5, the in-plane swing suppression gets worse while the out-plane swing suppression gets better with its increasing.

(3) The simulation tendencies follows the experiment curves quite well, and the variations between the experiment and simulation results are acceptable. Therefore, the dynamic modelling and analysis of CDITM are verified.

The three-dimensional dynamic model derived in this paper can be applied to predict the complex dynamic behavior of CDITM as well as be employed to optimize the engineering configuration of CDITM. The theoretical and experimental results are fundamental and valuable for the engineering application of CDITM in the offshore industries. Meanwhile, the research method of CDITM is a useful reference for other anti-swing mechanisms like RBTS.

REFERENCES

[1] J. J. Potter and W. E. Singhose, "Design and human-in-the-loop testing of reduced-modification input shapers," *IEEE Trans. Control Syst. Technol.*, vol. 24, no. 4, pp. 1513–1520, Jul. 2016.

[2] U. T. T. Hoang, H. X. Le, N. H. Thai, H. V. Pham, and L. Nguyen, "Consistency of control performance in 3D overhead cranes under payload mass uncertainty," *Electronics*, vol. 9, no. 4, p. 657, 2020.

[3] Z. Xu, Z. Wang, Z. Shen, and Y. Sun, "Nonlinear differential and integral sliding mode control for wave compensation system of ship-borne manipulator," *Meas. Control*, vol. 2020, Aug. 2020, Art. no. 002029402094495.

[4] N. Sun, Y. Fang, H. Chen, Y. Wu, and B. Lu, "Nonlinear antiswing control of offshore cranes with unknown parameters and persistent ship-induced perturbations: Theoretical design and hardware experiments," *IEEE Trans. Ind. Electron.*, vol. 65, no. 3, pp. 2629–2641, Mar. 2018.

[5] H. Chen and N. Sun, "Nonlinear control of underactuated systems subject to both actuated and unactuated state constraints with experimental verification," *IEEE Trans. Ind. Electron.*, vol. 67, no. 9, pp. 7702–7714, Sep. 2020.

[6] E. M. Abdel-Rahman, A. H. Nayfeh, and Z. N. Masoud, "Dynamics and control of cranes: A review," *J. Vib. Control*, vol. 9, no. 7, pp. 863–908, Jul. 2003.

[7] L. Ramli, Z. Mohamed, A. M. Abdullahi, H. I. Jaafar, and I. M. Lazim, "Control strategies for crane systems: A comprehensive review," *Mech. Syst. Signal Process.*, vol. 95, pp. 1–23, Oct. 2017.

[8] M. Yan, X. Ma, W. Bai, Z. Lin, and Y. Li, "Numerical simulation of wave interaction with payloads of different postures using OpenFOAM," *J. Mar. Sci. Eng.*, vol. 8, no. 6, p. 433, Jun. 2020.

[9] H. Chen and N. Sun, "An output feedback approach for regulation of 5-DOF offshore cranes with ship yaw and roll perturbations," *IEEE Trans. Ind. Electron.*, to be published.

[10] B. d' Andréa-Novel and J. M. Coron, "Exponential stabilization of an overhead crane with flexible cable via a back-stepping approach," *Automatica*, vol. 36, no. 4, pp. 587–593, Apr. 2000.

[11] B. d'Andra-Novel, F. Boustany, F. Conrad, and B. P. Rao, "Feedback stabilization of a hybrid PDE-ODE system: Application to an overhead crane," *Math. Control, Signals, Syst.*, vol. 7, no. 1, pp. 1–22, Mar. 1994.

[12] A. Aksjonov, V. Vodovozov, and E. Petlenkov, "Three-dimensional crane modelling and control using euler-Lagrange state-space approach and anti-swing fuzzy logic," *Electr., Control Commun. Eng.*, vol. 9, no. 1, pp. 5–13, Dec. 2015.

[13] M. H. Fatehi, M. Eghtesad, and R. Amjadifard, "Modelling and control of an overhead crane system with a flexible cable and large swing angle," *J. Low Freq. Noise, Vib. Active Control*, vol. 33, no. 4, pp. 395–409, Dec. 2014.

[14] V. Renuka and A. T. Mathew, "Precise modelling of a gantry crane system including friction 3d angular swing and hoisting cable flexibility," *Int. J. Theor. Appl. Res. Mech. Eng.*, vol. 2, pp. 119–125, Dec. 2013.

[15] W. Singhose, L. Porter, M. Kenison, and E. Kriikku, "Effects of hoisting on the input shaping control of gantry cranes," *Control Eng. Pract.*, vol. 8, no. 10, pp. 1159–1165, Oct. 2000.

[16] N. Sun, T. Yang, H. Chen, Y. Fang, and Y. Qian, "Adaptive anti-swing and positioning control for 4-DOF rotary cranes subject to uncertain/unknown parameters with hardware experiments," *IEEE Trans. Syst., Man, Cybern. Syst.*, vol. 49, no. 7, pp. 1309–1321, Jul. 2019.

[17] Y. G. Sun, H. Y. Qiang, J. Q. Xu, and D. S. Dong, "The nonlinera dynamics and anti-sway tracking control for offshore container crane on a mobile harbor," *J. Mar. Sci. Technol.-Taiwan, Process.*, vol. 25, no. 6, pp. 656–665, Dec. 2017.

[18] Y. Chu, V. Æsøy, S. Ehlers, and H. Zhang, "Integrated multi-domain system modelling and simulation for offshore crane operations," *Ship Technol. Res.*, vol. 62, no. 1, pp. 36–46, Feb. 2015.

[19] A. Sağirli, M. E. Bogoçlu, and V. E. Ömürlü, "Modeling the dynamics and kinematics of a telescopic rotary crane by the bond graph method: Part I," *Nonlinear Dyn.*, vol. 33, no. 4, pp. 337–351, Sep. 2003.

[20] A. Sağirli, M. E. Bogoçlu, and V. E. Ömürlü, "Modeling the dynamics and kinematics of a telescopic rotary crane by the bond graph method: Part II," *Nonlinear Dyn.*, vol. 33, no. 4, pp. 353–367, Sep. 2003.
[21] A. Cibicik and O. Egeland, "Dynamic modelling and force analysis of a knuckle boom crane using screw theory," *Mech. Mach. Theory*, vol. 133, pp. 179–194, Mar. 2019.
[22] J. Vaughan, D. Kim, and W. Singhose, "Control of tower cranes with double-pendulum payload dynamics," *IEEE Trans. Control Syst. Technol.*, vol. 18, no. 6, pp. 1345–1358, Nov. 2010.
[23] H. I. Jaafar, Z. Mohamed, M. A. Shamsudin, N. A. M. Subha, L. Ramli, and A. M. Abdullahi, "Model reference command shaping for vibration control of multimode flexible systems with application to a double-pendulum overhead crane," *Mech. Syst. Signal Process.*, vol. 115, pp. 677–695, Jan. 2019.
[24] W. Singhose, D. Kim, and M. Kenison, "Input shaping control of double-pendulum bridge crane oscillations," *J. Dyn. Syst., Meas., Control*, vol. 130, no. 3, May 2008, Art. no. 034504.
[25] N. Sun, Y. Fang, H. Chen, and B. Lu, "Amplitude-saturated nonlinear output feedback antiswing control for underactuated cranes with double-pendulum cargo dynamics," *IEEE Trans. Ind. Electron.*, vol. 64, no. 3, pp. 2135–2146, Mar. 2017.
[26] E. Maleki and W. Singhose, "Swing dynamics and input-shaping control of human-operated double-pendulum boom cranes," *J. Comput. Nonlinear Dyn.*, vol. 7, no. 3, Jul. 2012, Art. no. 031006.
[27] J. Neupert, T. Heinze, O. Sawodny, and K. Schneider, "Observer design for boom cranes with double-pendulum effect," in *Proc. ISIC*, Jul. 2009, pp. 1545–1550.
[28] J. Huang, Z. Liang, and Q. Zang, "Dynamics and swing control of double-pendulum bridge cranes with distributed-mass beams," *Mech. Syst. Signal Process.*, vols. 54–55, pp. 357–366, Mar. 2015.
[29] J. Huang, X. Xie, and Z. Liang, "Control of bridge cranes with distributed-mass payload dynamics," *IEEE/ASME Trans. Mechatronics*, vol. 20, no. 1, pp. 481–486, Feb. 2015.
[30] R. Tang and J. Huang, "Control of bridge cranes with distributed-mass payloads under windy conditions," *Mech. Syst. Signal Process.*, vols. 72–73, pp. 409–419, May 2016.
[31] Y. M. Al-Sweiti and D. Söffker, "Planar cargo control of elastic ship cranes with the 'maryland rigging' system," *J. Vib. Control*, vol. 13, no. 3, pp. 241–267, 2007.
[32] B. Kimiaghalam, A. Homaifar, and M. Bikdash, "Feedback and feedforward control law for a ship crane with maryland rigging system," in *Proc. Amer. Control Conf.*, 2000, pp. 1047–1051.
[33] B. Kimiaghalam, A. Homaifar, M. Bikdash, and B. R. Hunt, "Feedforward control law for a shipboard crane with maryland rigging system," *J. Vib. Control*, vol. 8, no. 2, pp. 159–188, Feb. 2002.
[34] N.-K. Ku, J.-H. Cha, M.-I. Roh, and K.-Y. Lee, "A tagline proportional–derivative control method for the anti-swing motion of a heavy load suspended by a floating crane in waves," *Proc. Inst. Mech. Eng., M, J. Eng. Maritime Environ.*, vol. 227, no. 4, pp. 357–366, Nov. 2013.
[35] G. Parker, M. Graziano, F. Leban, J. Green, and J. D. Bird, "Reducing crane payload swing using a rider block tagline control system," in *Proc. OCEANS*, Aberdeen, Scotland, Oct. 2007, pp. 1–5.
[36] B. Wen, A. Homaifar, M. Bikdash, and B. Kimiaghalam, "Modeling and optimal control design of shipboard crane," in *Proc. Amer. Control Conf.*, San Diego, CA, USA, vol. 1, 1999, pp. 593–597.
[37] J. Ginsberg, *Engineering Dynamics*. New York, NY, USA: Cambridge Univ. Press, 2008, pp. 99–157.

SHENGHAI WANG received the Ph.D. degree in marine engineering from Dalian Maritime University, Dalian, China, in 2018.

He is currently a Lecturer with the College of Marine Engineering, Dalian Maritime University. His research interests include cable-driven parallel robots, anti-swing technology of shipboard crane, and development and research of marine and ocean engineering equipment.

ZHAOPENG REN received the M.E. degree in marine engineering from Dalian Maritime University, Dalian, China, in 2019, where he is currently pursuing the Ph.D. degree in marine engineering.

His research interest includes optimal design and dynamic control of shipboard crane.

GUOLIANG JIN received the B.E. degree from the College of Marine Engineering, Dalian Maritime University, Dalian, China, in 2019, where he is currently pursuing the master's degree in marine engineering.

His research interests include anti-swing technology and dynamic control of marine crane.

HAIQUAN CHEN received the M.E. degree from the College of Marine Engineering, Dalian Maritime University, Dalian, China, in 1996.

He is currently a Professor with the College of Marine Engineering, Dalian Maritime University. His research interests include advanced marine hydraulic control, anti-swing technology of marine crane, and development and research of marine and ocean engineering equipment.